Volume 45 | Number 30 | 14 August 2016 | Pages 11913–12238

Dalton Transactions

An international journal of inorganic chemistry

www.rsc.org/dalton

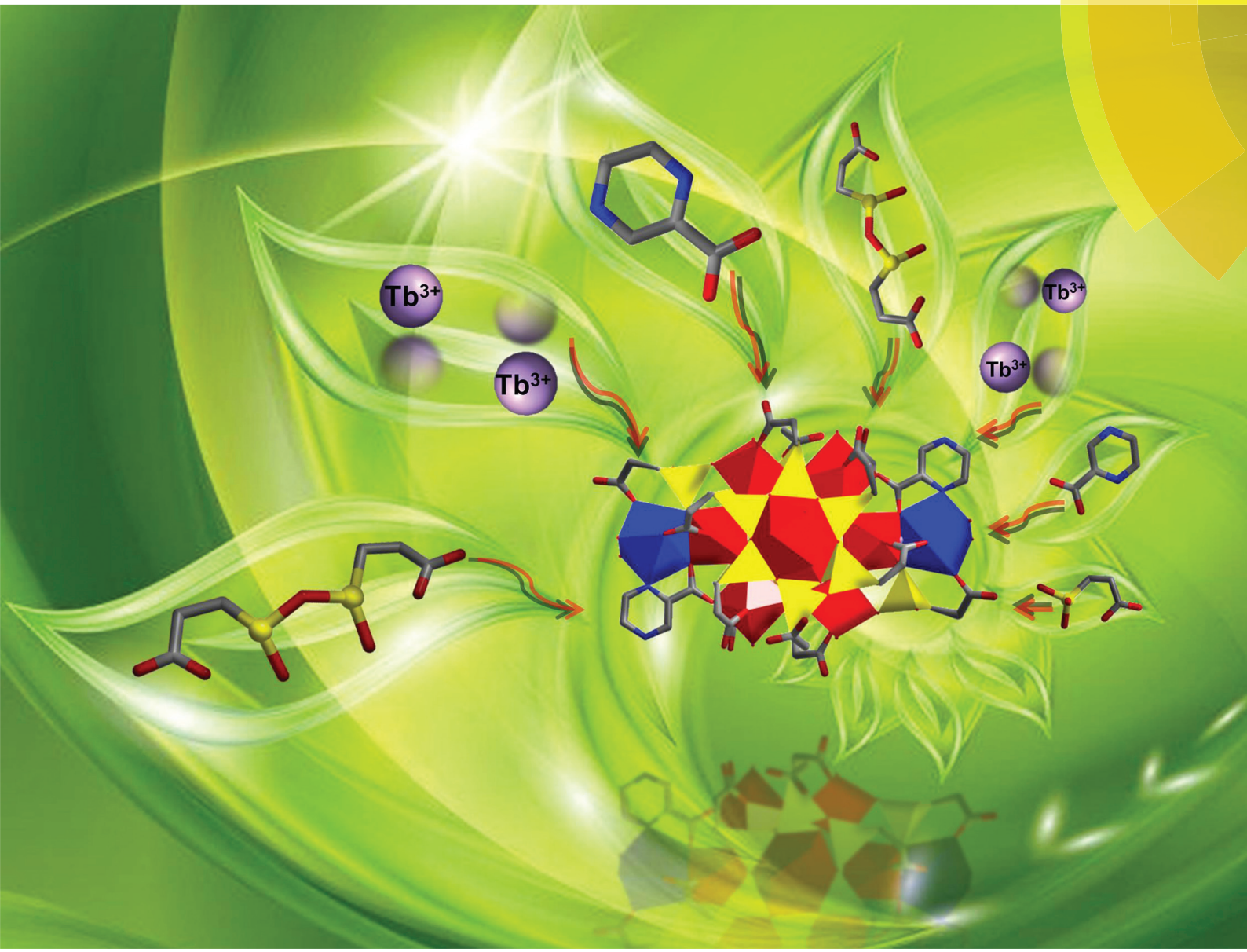

ISSN 1477-9226

ROYAL SOCIETY OF CHEMISTRY

PAPER

Jun-Wei Zhao, Guo-Yu Yang *et al.*

A series of lanthanide germanate cluster organic frameworks

175 YEARS

Dalton Transactions

PAPER

View Article Online
View Journal | View Issue

Cite this: *Dalton Trans.*, 2016, **45**, 11958

A series of lanthanide germanate cluster organic frameworks†

Lei-Lei Li,[a] Rui Pan,[a] Jun-Wei Zhao,*[b] Bai-Feng Yang[a] and Guo-Yu Yang*[a,c]

Received 27th April 2016,
Accepted 24th May 2016

DOI: 10.1039/c6dt01629d

www.rsc.org/dalton

Six new lanthanide (Ln) germanate cluster organic frameworks (LnGeCOFs) derived from $\{Ln_8Ge_{12}\}$ cage cluster units $\{[Nd(pza)_2(H_2O)]$ $[Nd_8Ge_{12}(\mu_3\text{-}O)_{24}E_{12}(pza)(H_2O)_{12}]\}\cdot 3H_2O$ (**1**), $\{[Dy(CH_3COO)(CO_3)(H_2O)]_2[Dy_8Ge_{12}(\mu_3\text{-}O)_{24}E_{12}(H_2O)_{12}]\}\cdot 11H_2O$ (**2**), $\{[TbGeE(HO)_2O(pza)\ (H_2O)]_2[Tb_8Ge_{12}(\mu_3\text{-}O)_{24}E_{12}(H_2O)_6]\}\cdot 18H_2O$ (**3**), $\{[DyGeE(HO)_2O(C_3H_5NO_2)(H_2O)]_2[Dy_8Ge_{12}(\mu_3\text{-}O)_{24}E_{12}(H_2O)_8]\}\cdot 8H_2O$ (**4**), $\{[Tb(pca)_2\ (H_2O)]_3[Tb_8Ge_{12}(\mu_3\text{-}O)_{24}E_{12}(H_2O)_4]\}\cdot(OH)_3\cdot 10H_2O$ (**5**) and $\{[Dy(pza)_2(H_2O)][Dy(pza)_2(H_2O)_2][Dy(pza)_3(H_2O)][Dy_8Ge_{12}(\mu_3\text{-}O)_{24}E_{12}(pza)(HCOO)\ (H_2O)_6]\}\cdot 5H_2O$ (**6**) have been hydrothermally synthesized and structurally characterized. Increasing the amount of the second ligands can induce not only the assembly from **1** to **5**, **6** based on Ln oxides as the starting sources, but also the assembly from **2** to **3**, **4** based on Ln salts as the starting sources. The successful preparation of these LnGeCOFs suggests the importance of the second ligands in the structural construction of **1–6**. To our knowledge, **1** is the first example that includes right- and left-handed helical chains among LnGeCOFs based on bis(carboxyethylgermanium) sesquioxide. **2**, **4** and **6** are the first dysprosium incorporated organogermanates based on bis(carboxyethylgermanium)sesquioxide. **4** and **5** display very open framework structures with a solvent-accessible volume of 34.6% for **4** and 35.0% for **5**. Moreover, the solid-state photoluminescence properties of **1**, **3** and **5** have been investigated at room temperature and they exhibit the characteristic emission bands derived from Ln cations.

Introduction

Open-framework materials with an increasing pore size and decreasing framework density have spurred increasing interest due to their rich structural chemistry and potential applications in selective catalysis, ion exchange, adsorption and separation.[1] Open-framework materials with extra-large pores are often observed in aluminosilicates,[2] phosphates,[3] and germanates.[4] Among all these materials, germanates with open frameworks have attracted particular attention because of their unique structural architectures and interesting properties. However the synthesis of open-framework germanates with a low framework density remains a challenging research field. An alternative strategy of replacing the nodes of a simple underlying net with polyatomic structural building units (SBUs) has been brought up by Férey, O'Keeffe and Yaghi in the concept of scale chemistry.[5] This strategy is particularly fruitful for designing open-framework germanates with unique properties, because germanium can generate GeO_4 tetrahedra, GeO_5 trigonal bipyramids and GeO_6 octahedra as a result of its larger coordination sphere, which tend to form typical cluster building units.[4c,6–9] A notable example is SU-M with extra-large 30-ring channels that is built by Ge_{10} clusters.[4a]

Recently, considerable attention has been paid to preparing microporous germanates and investigating the effect of the introduced heteroatoms on their frameworks. Interestingly, the incorporation of Ln ions into the skeletons of germanates leads to novel porous Ln germanates (LnGes) with diverse architectural features and intriguing luminescence and magnetic properties. However, LnGes, especially open framework LnGes, remain less explored and the synthetic methods are mainly limited to the flux-growth and high-temperature/high-pressure hydrothermal conditions. For example, in 2002, Emirdag-Eanes *et al.* prepared $NaSm_3(GeO_4)_2(OH)_2$ under high-temperature/high-pressure conditions.[10] In 2008, Chen's group reported a $KEuGe_2O_6$ with parallel zigzag chains of edge-sharing Eu–O polyhedra by both flux-growth and high-temperature/high-pressure hydrothermal methods and studied

[a]*MOE Key Laboratory of Cluster Science, School of Chemistry, Beijing Institute of Technology, Beijing 100081, China. E-mail: ygy@bit.edu.cn*
[b]*Henan Key Laboratory of Polyoxometalate Chemistry, College of Chemistry and Chemical Engineering, Henan University, Kaifeng, Henan 475004, China. E-mail: zhaojunwei@henu.edu.cn*
[c]*Department of Chemistry, Key Laboratory for Preparation and Application of Ordered Structural Materials of Guangdong Province, Shantou University, Shantou, Guangdong 515063, China*

†Electronic supplementary information (ESI) available: Refinement details and additional figures. CCDC 1443704–1443706, 1470855, 1470201 and 1443708. For ESI and crystallographic data in CIF or other electronic format see DOI: 10.1039/c6dt01629d

the room-temperature emission behavior.[11] In 2014, Liu *et al.* obtained a family of 2D-layered LnGes $K_3[Gd_{1-x}Tb_xGe_3O_8(OH)_2]$ (x = 0, 0.3, 0.1, 1) by high-temperature/high-pressure hydrothermal methods and intensively investigated the efficient $Gd^{III} \rightarrow Tb^{III}$ energy transfer.[12] But only a few LnGes have been prepared under mild hydrothermal environments to date. For instance, in 2012, Xu's group prepared a high-pressure stable photoluminescence Eu-containing germanate $NaEu_3(GeO_4)_2(OH)_2$ and a family of LnGes $K_3[Tb_xEu_{1-x}Ge_3O_8(OH)_2]$ (x = 1, 0.88, 0.67, 0) with tunable photoluminescence properties by a mild hydrothermal method.[13] It is worth mentioning that preparing open framework LnGes under mild hydrothermal conditions is still a challenge. To obtain open framework LnGes under mild hydrothermal conditions, we introduce another type of germanium source, bis(carboxyethylgermanium)sesquioxide, $(HOOCCH_2CH_2)_2Ge_2O_3$ ($H_2E_2Ge_2O_3$, E = $-CH_2CH_2COO-$) as a starting material to prepare LnGes based on the following reasons: (i) Ln ions are hard acids and preferentially bind to hard (O-donor) atoms.[14] $H_2E_2Ge_2O_3$ containing two carboxyl groups and a Ge_2O_3 (O═Ge–O–Ge═O) core with two Ge═O bonds can easily arrest Ln ions and the opening of Ge═O bonds in the Ge_2O_3 core can polymerize to form Ge–O clusters and Ge–O chain/layers, thus the carboxyl groups and the Ge_2O_3 core offer the potential possibility for the formation of expanded frameworks; (ii) little attention has been paid to exploit the systematic reactions between Ln complexes and $H_2E_2Ge_2O_3$ except for FJ-19 and FJ-20 synthesized by our group.[15] Herein, we report six new LnGes $\{[Nd(pza)_2(H_2O)][Nd_8Ge_{12}(\mu_3\text{-}O)_{24}E_{12}(pza)(H_2O)_{12}]\}\cdot 3H_2O$ (**1**), $\{[Dy(CH_3COO)(CO_3)(H_2O)]_2[Dy_8Ge_{12}(\mu_3\text{-}O)_{24}E_{12}(H_2O)_{12}]\}\cdot 11H_2O$ (**2**), $\{[TbGeE(HO)_2O(pza)(H_2O)]_2\ [Tb_8Ge_{12}(\mu_3\text{-}O)_{24}E_{12}(H_2O)_6]\}\cdot 18H_2O$ (**3**), $\{[DyGeE(HO)_2O(C_3H_5NO_2)(H_2O)]_2[Dy_8Ge_{12}(\mu_3\text{-}O)_{24}E_{12}(H_2O)_8]\}\cdot 8H_2O$ (**4**), $\{[Tb(pca)_2(H_2O)]_3\ [Tb_8Ge_{12}(\mu_3\text{-}O)_{24}E_{12}(H_2O)_4]\}\cdot (OH)_3\cdot 10H_2O$ (**5**) and $\{[Dy(pza)_2(H_2O)]\ [Dy(pza)_2(H_2O)_2][Dy(pza)_3(H_2O)][Dy_8Ge_{12}(\mu_3\text{-}O)_{24}E_{12}(pza)(HCOO)\ (H_2O)_6]\}\cdot 5H_2O$ (**6**) (Hpza = 2-pyrazinecarboxylic acid, Hpca = 2-picolinic acid) that were prepared by the mild hydrothermal method. Intriguingly, six novel organic–inorganic hybrid LnGes are derived from bicapped sandwich-type cage clusters, $\{Nd_9Ge_{12}(\mu_3\text{-}O)_{24}E_{12}\}$ ($\{Nd_9Ge_{12}\}$), $\{Dy_{10}Ge_{12}(\mu_3\text{-}O)_{24}E_{12}\}$ ($\{Dy_{10}Ge_{12}\}$), $\{Ln_{10}Ge_{14}(\mu_3\text{-}O)_{24}E_{12}\}$ ($\{Ln_{10}Ge_{14}\}$, Ln = Tb/Dy), and $\{Ln_{11}Ge_{12}(\mu_3\text{-}O)_{24}E_{12}\}$ ($\{Ln_{11}Ge_{12}\}$, Ln = Tb/Dy). The second ligands play an important role in constructing **1–6** and the amount of the second ligands can induce the assembly from $\{Nd_9Ge_{12}\}$-**1** to $\{Ln_{11}Ge_{12}\}$-**5**, **6** (Ln = Tb^{3+}, **5**; Dy^{3+}, **6**) and from $\{Dy_{10}Ge_{12}\}$-**2** to $\{Ln_{10}Ge_{14}\}$-**3**, **4** (Ln = Tb^{3+}, **3**; Dy^{3+}, **4**). Notably, **1** represents the first LnGes with right- and left-handed helical chains. **2**, **4** and **6** are the first Dy-containing germanates based on $H_2E_2Ge_2O_3$. **4** and **5** display very open frameworks with a solvent-accessible volume of 34.6% for **4** and 35.0% for **5**. The luminescence properties of **1**, **3** and **5** have also been probed, showing that **1** displays the characteristic emission bands of the Nd^{3+} cations with transitions from the $^4F_{3/2}$ excited-state to lower ^4I_J (J = 9/2, 11/2, and 13/2) levels, and **3** and **5** exhibit the green luminescence mainly originating from the $^5D_4 \rightarrow {}^7F_5$ transition of the Tb^{3+} cations. All of these suggest that they may be suitable as potential candidates for fluorescent materials.

Experimental

Materials and physical measurements

All chemicals were purchased commercially and used without further purification. Powder X-ray diffraction (PXRD) data were collected on a Bruker D8 Advance diffractometer with Cu Kα radiation (λ = 1.5406 Å). Elemental analyses for C, H and N were performed on a Euro EA 3000 CHNS/O analyzer. FT-IR spectra were obtained on a Smart Omni Transmission spectrophotometer with KBr pellets in the range of 4000–500 cm^{-1}. Thermogravimetric (TG) analyses were carried out on a Mettler TGA/SDTA 851 thermal analyzer in the temperature range of 30–1000 °C in an air atmosphere with a heating rate of 10 °C min^{-1}. Luminescence measurements were performed in the solid state at room temperature with an Edinburgh FLS920 fluorescence spectrometer.

Preparations of 1–6

$\{[Nd(pza)_2(H_2O)][Nd_8Ge_{12}(\mu_3\text{-}O)_{24}E_{12}(pza)(H_2O)_{12}]\}\cdot 3H_2O$ (1). A mixture of $H_2E_2Ge_2O_3$ (0.084 g, 0.247 mmol) and Nd_2O_3 (0.084 g, 0.253 mmol) was stirred in H_2O (10 mL, 556 mmol) for 30 min, and Hpza (0.062 g, 0.500 mmol) and $HClO_4$ (0.025 g, 0.250 mmol) were added. The resulting mixture was stirred for 30 min (pH 2), sealed in a 40 mL Teflon-lined bomb, kept at 170 °C for 7 days, and then cooled to room temperature. Pink block crystals of **1** suitable for X-ray diffraction were obtained by filtration, washed with distilled water, and dried in air. Yield: 57% for **1** based on $H_2E_2Ge_2O_3$. Anal. calcd (%) for **1**, $C_{51}H_{89}N_6O_{70}Ge_{12}Nd_9$: C, 15.03; H, 2.20; N, 2.06. Found: C, 14.89; H, 2.14; N, 1.96. IR (KBr, cm^{-1}): 3413s, 2967w, 2928w, 1583vs, 1431m, 1386m, 1294w, 1255w, 1159w, 1034w, 769vs, 719m, 605w, 520m (Fig. S1†).

$\{[Dy(CH_3COO)(CO_3)(H_2O)]_2[Dy_8Ge_{12}(\mu_3\text{-}O)_{24}E_{12}(H_2O)_{12}]\}\cdot 11H_2O$ (2). A mixture of $H_2E_2Ge_2O_3$ (0.084 g, 0.247 mmol), $Dy(CH_3COO)_3\cdot 4H_2O$ (0.108 g, 0.262 mmol) and Na_2CO_3 (0.025 g, 0.236 mmol) was stirred in H_2O (10 mL, 556 mmol) for 30 min (pH 6), sealed in a 40 mL Teflon-lined bomb at 170 °C for 7 days and cooled to room temperature. Colorless block crystals of **2** suitable for X-ray diffraction were obtained by filtration, washed with distilled water and dried in air. Yield: 32% for **2** based on $H_2E_2Ge_2O_3$. Anal. calcd (%) for **2**, $C_{42}H_{104}O_{83}Ge_{12}Dy_{10}$: C, 11.38; H, 2.36. Found: C, 11.30; H, 2.35. IR (KBr, cm^{-1}): 3420s, 2967w, 2922w, 1594vs, 1509w, 1436w, 1380s, 1294w, 1159m, 764s, 611w, 543w (Fig. S1†).

$\{[TbGeE(HO)_2O(pza)(H_2O)]_2[Tb_8Ge_{12}(\mu_3\text{-}O)_{24}E_{12}(H_2O)_6]\}\cdot 18H_2O$ (3). A mixture of $H_2E_2Ge_2O_3$ (0.084 g, 0.247 mmol), $Tb(NO_3)_3\cdot 6H_2O$ (0.206 g, 0.455 mmol) and 1,2-diaminopropane (0.019 g, 0.256 mmol) was stirred in H_2O (10 mL, 556 mmol) for 30 min (pH 6), and then Hpza (0.031 g, 0.250 mmol) was added. The resulting mixture was stirred for 30 min, sealed in a 40 mL Teflon-lined bomb at 170 °C for 7 days and cooled to room temperature. Colorless block crystals of **3** suitable for X-ray

diffraction were obtained by filtration, washed with distilled water, and dried in air. Yield: 41% for **3** based on $H_2E_2Ge_2O_3$. Anal. calcd (%) for **3**, $C_{51}H_{118}N_4O_{88}Ge_{14}Tb_{10}$: C, 12.76; H, 2.48; N, 1.17. Found: C, 12.72; H, 2.43; N, 1.16. IR (KBr, cm^{-1}): 3426s, 2962w, 2918w, 1600vs, 1442m, 1386m, 1307w, 1159w, 1052w, 1017w, 768vs, 707m, 623w, 543m (Fig. S1†).

$\{[DyGeE(HO)_2O(C_3H_5NO_2)(H_2O)]_2[Dy_8Ge_{12}(\mu_3\text{-}O)_{24}E_{12}(H_2O)_8]\}\cdot 8H_2O$ (4). A mixture of $H_2E_2Ge_2O_3$ (0.084 g, 0.247 mmol), $Dy(CH_3COO)_3\cdot 4H_2O$ (0.206 g, 0.500 mmol) and 1,2-diaminopropane (0.019 g, 0.256 mmol) was stirred in H_2O (10 mL, 556 mmol) for 30 min (pH 6) and then DL-tyrosine (0.091 g, 0.502 mmol) was added. The resulting mixture was stirred for 30 min, sealed in a 40 mL Teflon-lined bomb at 170 °C for 7 days and cooled to room temperature. Colorless block crystals of **4** suitable for X-ray diffraction were obtained by filtration, washed with distilled water, and dried in air. Yield: 48% for **4** based on $H_2E_2Ge_2O_3$. Anal. calcd (%) for **4**, $C_{48}H_{106}N_2O_{80}Ge_{14}Dy_{10}$: C, 12.44; H, 2.30; N, 0.60. Found: C, 12.42; H, 2.20; N, 0.57. IR (KBr, cm^{-1}): 3426s, 2962w, 2922w, 1571vs, 1436m, 1386m, 1306w, 1249w, 1159m, 1069w, 978w, 764vs, 713m, 623w, 549m (Fig. S1†).

$\{[Tb(pca)_2(H_2O)]_3[Tb_8Ge_{12}(\mu_3\text{-}O)_{24}E_{12}(H_2O)_4]\}\cdot(OH)_3\cdot 10H_2O$ (5). A mixture of $H_2E_2Ge_2O_3$ (0.150 g, 0.446 mmol) and Tb_4O_7 (0.074 g, 0.099 mmol) was stirred in H_2O (10 mL, 556 mmol) for about 5 min and then Hpca (0.124 g, 1.007 mmol) and $HClO_4$ (0.077 g, 0.770 mmol) were added. The resulting mixture was stirred for 30 min (pH 2), sealed in a 40 mL Teflon-lined bomb at 170 °C for 7 days and cooled to room temperature. Colorless prismatic crystals of **5** were obtained by filtration, washed with distilled water and dried in air. Yield: 52% for **5** based on $H_2E_2Ge_2O_3$. Anal. calcd (%) for **5**, $C_{72}H_{109}N_6O_{80}Ge_{12}Tb_{11}$: C, 17.44; H, 2.22; N, 1.69. Found: C, 17.38; H, 2.16; N, 1.64. IR (KBr, cm^{-1}): 3426s, 2967w, 2928w, 1639s, 1588vs, 1560s, 1431m, 1380m, 1300w, 1249w, 1159w, 1097w, 1051w, 1017w, 764vs, 702m, 617w, 537w (Fig. S1†).

$\{[Dy(pza)_2(H_2O)][Dy(pza)_2(H_2O)_2][Dy(pza)_3(H_2O)][Dy_8Ge_{12}(\mu_3\text{-}O)_{24}E_{12}(pza)(HCOO)(H_2O)_6]\}\cdot 5H_2O$ (6). A mixture of $H_2E_2Ge_2O_3$ (0.078 g, 0.232 mmol), Dy_2O_3 (0.093 g, 0.249 mmol), Hpza (0.140 g, 1.128 mmol) and $HCOONa\cdot 2H_2O$ (0.026 g, 0.25 mmol) was stirred in H_2O (10 mL, 556 mmol) for 30 min (pH 3), sealed in a 40 mL Teflon-lined bomb at 170 °C for 7 days and cooled to room temperature. Colorless block crystals of **6** suitable for X-ray diffraction were obtained by filtration, washed with distilled water and dried in air. Yield: 43% for **6** based on $H_2E_2Ge_2O_3$. Anal. calcd (%) for **6**, $C_{77}H_{103}N_{16}O_{81}Ge_{12}Dy_{11}$: C, 17.76; H, 1.99; N, 4.30. Found: C, 17.73 H, 1.95; N, 4.26. IR (KBr, cm^{-1}): 3414s, 2957w, 1633s, 1588vs, 1431m, 1380m, 1294w, 1165m, 1035m, 860w, 769vs, 606w, 532m (Fig. S1†).

X-ray crystallography

The intensity data collection of **1–6** was performed on Gemini A Ultra diffractometer using graphite-monochromated Mo Kα (λ = 0.71073 Å) at 293(2) K. Their structures were solved by the direct methods and refined on F^2 and Fourier syntheses were performed by full-matrix least-squares methods using the SHELXTL 97 program package.[16] Lorentz polarization and empirical absorption correction were applied. All hydrogen atoms attached to carbon and nitrogen atoms were geometrically placed and refined isotropically as a riding model using the default SHELXTL parameters. No hydrogen atoms associated with water molecules were located from the difference Fourier map. All non-hydrogen atoms were refined anisotropically (the refinement details for **1–6** are given in the ESI†). Crystallographic data and structural refinements for **1–6** are summarized in Table 1. Crystallographic data for this paper have been deposited at the Cambridge Crystallographic Data Centre with CCDC 1443704–1443706, 1470855, 1470201, and 1443708 for **1–6**, respectively.

Results and discussion

Structural description

1 crystallizes in the orthorhombic crystal system with a space group of *Fdd*2. It consists of one independent $\{Nd_9Ge_{12}\}$-**1** SBU (Fig. S2 in the ESI†), which is constructed from one bicapped sandwich-type $\{Nd_8Ge_{12}\}$ cage cluster and one supporting $[Nd(pza)_2(H_2O)]^+$ unit through two O_{COO} atoms from two E groups and two O_{COO} atoms from two pza ligands (Fig. 1a–e). The $\{Nd_8Ge_{12}\}$ cage can also be visualized as two face-to-face Ge_6 rings sandwiching one hexagon Nd_6 ring by twelve carboxyl μ_2-O_{COO} atoms from twelve E groups and twelve exotic μ_3-O atoms originating from the opening of twelve Ge=O double bonds and further capped by two $\{NdO_{10}\}$ polyhedra through six μ_3-O atoms. In both Ge_6 rings, all the Ge centers utilize the four-coordinate $\{GeO_3C\}$ tetrahedra (Fig. S3a–c in the ESI†): two O_{Ge} atoms from the Ge_2O_3 cores of the $E_2Ge_2O_3^{2-}$ moieties and one exotic O_{Ge} atom from the polymeric process of the Ge_2O_3 core. The Ge–C and Ge–O distances are in the range of 1.899(10)–1.955(9) Å and 1.728(7)–1.821(7) Å, respectively. All the bond lengths are in agreement with the previously reported values.[15] Six $\{GeO_3C\}$ tetrahedra are connected together in a corner-sharing fashion to create the planar Ge_6 ring. The E groups linking both Ge_6 rings bend to the opposite directions in the basal plane. Six equatorial Nd^{3+} cations in the Nd_6 ring are all eight-coordinate and display the distorted bicapped trigonal prism geometries (Fig. S3d–l in the ESI†), in which two $E_2Ge_2O_3^{2-}$ moieties as tridentate ligands chelate two sides of each Nd^{3+} cation *via* two O_{Ge} atoms and one O_{COO} atom of each $E_2Ge_2O_3^{2-}$ moiety and the remaining two sites are occupied by one terminal water molecule and one O_{COO} atom of the pza ligand ($Nd1^{3+}$, $Nd2^{3+}$, $Nd3^{3+}$ and $Nd5^{3+}$), two terminal water molecules ($Nd4^{3+}$) or two O_{COO} atoms of the pza ligands ($Nd6^{3+}$). The six equatorial $\{NdO_8\}$ polyhedra are connected in the edge-sharing mode to form the Nd_6 6-ring. Each of the two capped Nd^{3+} cations ($Nd7^{3+}$/$Nd8^{3+}$) at two polar positions of the $\{Nd_8Ge_{12}\}$ cage is coordinated by six μ_3-O_{Ge} atoms from the Ge_6 ring, one O_{COO} atom of one E group and three terminal water molecules and completes the ten-coordinate monocapped triangular cupola geometry (Fig. S3m–o in the ESI†), which is different from that

Table 1 Crystallographic data and structural refinements of **1–6**

	1	2	3	4	5	6
Formula	$C_{51}H_{89}N_6O_{70}Ge_{12}Nd_9$	$C_{42}H_{104}O_{83}Ge_{12}Dy_{10}$	$C_{52}H_{118}N_4O_{88}Ge_{14}Tb_{10}$	$C_{48}H_{106}N_2O_{80}Ge_{14}Dy_{10}$	$C_{72}H_{109}N_6O_{80}Ge_{12}Tb_{11}$	$C_{77}H_{103}N_{16}O_{81}Ge_{12}Dy_{11}$
Fw	4076.09	4433.33	4812.96	4630.59	4957.85	5207.33
Crystalsystem	Orthorhombic	Monoclinic	Triclinic	Monoclinic	Cubic	Orthorhombic
Space group	*Fdd2*	$P2_1/c$	$P\bar{1}$	$P2_1/c$	*I*43*m*	$P2_12_12_1$
a, Å	29.8951(4)	14.7192(3)	12.8712(2)	18.8542(5)	31.9966(2)	19.3746(2)
b, Å	87.9118(12)	16.5170(3)	21.6552(4)	18.0734(5)	31.9966(2)	21.4307(3)
c, Å	16.0433(2)	21.7274(5)	23.5052(4)	19.5409(7)	31.9966(2)	33.7110(4)
α, °	90	90	106.275(2)	90	90	90
β, °	90	94.451(2)	101.460(2)	94.771(3)	90	90
γ, °	90	90	94.9090(10)	90	90	90
V, Å^3	42 163.9(10)	5266.37(19)	6093.78(18)	6635.7(3)	32 757.6(4)	13 997.2(3)
Z	16	2	2	2	8	4
D_c, g cm^{-3}	2.568	2.796	2.623	2.319	2.011	2.471
T, K	293(2)	293(2)	293(2)	293(2)	293(2)	293(2)
F(000)	30 736	4128	4520	4312	18 576	9740
μ, mm^{-1}	7.813	10.474	9.220	8.758	6.925	8.426
Reflections collected/unique	10 927/26 356	35 352/9257	69 065/23 923	34 386/11 681	14 823/5010	58 456/23 439
R_{int}	0.0422	0.0410	0.0325	0.0695	0.0318	0.0347
GOF on F^2	1.071	1.045	1.013	1.052	1.048	1.040
R_1, wR_2 ($I > 2\sigma(I)$)[a]	0.0440, 0.1297	0.0421, 0.0989	0.0260, 0.0590	0.0808, 0.2102	0.0444, 0.1202	0.0354, 0.0931
R_1, wR_2 (all data)	0.0505, 0.1367	0.0521, 0.1024	0.0365, 0.0629	0.1312, 0.2755	0.0520, 0.1268	0.0407, 0.0964

[a] $R_1 = \sum||F_o| - |F_c||/\sum|F_o|$, w$R_2 = [\sum w(F_o^2 - F_c^2)^2/\sum w(F_o^2)^2]^{1/2}$.

Fig. 1 (a) View of the $[Nd(pza)_2(H_2O)]^+$ cation. (b) Top view of the bicapped sandwich-type $\{Nd_8Ge_{12}\}$ cluster. (c) The pza ligand linking the $[Nd(pza)_2(H_2O)]^+$ cation. (d, e) Top and side views of the $\{Nd_9Ge_{12}\}$-**1** SBU in **1**. (f, g) The linking modes of adjacent $\{Nd_9Ge_{12}\}$-**1** SBUs in **1**. (h) The combination mode of each $\{Nd_9Ge_{12}\}$-**1** SBU with neighboring SBUs. The light blue balls represent adjacent $\{Nd_9Ge_{12}\}$-**1** SBU. (i) View of the 3D structure of **1** along the [101] direction. (j) Schematic topological view of the 3D framework of **1**. (k) View of the 2D layer constructed by right- and left-handed helical chains. (l, m) Schematic topological view of the 2D layer including right- and left-handed helical chains.

of capped Nd^{3+} cations in the previously reported FJ-19 prepared by our group.[15] As for the supporting Nd^{3+} cation ($Nd9^{3+}$), it displays the eight-coordinate bicapped trigonal prism geometry defined by three O_{COO} atoms of E groups, two N atoms and two O_{COO} atoms of pza ligands and one terminal water molecule (Fig. S3p–r in the ESI†). The Nd–O distances range from 2.275(7) to 2.745(7) Å and the Nd–N distances vary from 2.660(10) to 2.720(11) Å. Here, the second pza ligands play an important role in preparing and stabilizing the $\{Nd_9Ge_{12}\}$-**1** SBU and adopt two types of coordination modes in **1** (Fig. S4 in the ESI†): one acts as the connector between the bicapped sandwich-type $\{Nd_8Ge_{12}\}$ cage cluster and the supporting $\{NdN_2O_7\}$ polyhedron in the μ_3-η^1:η^2:η^1 mode; the other links two adjacent equatorial Nd^{3+} cations *via* two O_{COO} atoms. In **1**, the bridges between adjacent $\{Nd_9Ge_{12}\}$-**1** SBUs are E groups and adopt two kinds of linking modes: the single-armed shoulder-to-shoulder mode and the single-armed face-to-head mode (Fig. 1f and g). Intriguingly, each $\{Nd_9Ge_{12}\}$-**1** SBU links six same ones to form the 3D structure with 2D channels along the [101] and [001] directions (Fig. 1h, i and S5 in the ESI†). From the topological viewpoint, the whole 3D structure can be viewed as a 6-connected framework

with the Schläfli symbol of $(3^3{\cdot}4^4{\cdot}5^3{\cdot}6^5)$ by considering each $\{Nd_9Ge_{12}\}$-**1** SBU as a 6-connected node (Fig. 1j). It is worth mentioning that the whole structure of **1** consists of 2D layers built from right- and left-handed helical chains (Fig. 1k–m). As far as we know, it represents the first example including right- and left-handed helical chains among LnGes based on $H_2E_2Ge_2O_3$.

Since Ln salts have a better solubility in water than Ln oxides, they can react better with $H_2E_2Ge_2O_3$ under hydrothermal conditions. Therefore, we used Ln salts as the Ln sources with the aim of preparing more unique structures with larger SBUs. Using Na_2CO_3 to adjust the pH of the reaction system, we obtained **2** including a $\{Dy_{10}Ge_{12}\}$-**2** SBU, which consists of two equivalently related $\{Dy_5Ge_6\}$ half-units (Fig. S6 in the ESI†) by an inversion center with the atomic coordinate of (0.5, 0.5, 0.5). The centrosymmetrical $\{Dy_{10}Ge_{12}\}$-**2** SBU is formed *via* corner-sharing between one bicapped sandwich-type $\{Dy_8Ge_{12}\}$ cage and two supporting $[Dy(CH_3COO)(CO_3)(H_2O)]$ moieties *via* two O atoms from two E groups and two O atoms from one CO_3^{2-} moiety (Fig. 2a–d). Beyond our expectation, the CO_3^{2-} anions not only adjust the pH of the reaction system, but also act as the second ligand connecting the $\{Dy_8Ge_{12}\}$ cage with two supporting $[Dy(CH_3{-}COO)(CO_3)(H_2O)]$ moieties in the $\mu_3{-}\eta^1{:}\eta^2{:}\eta^1$ mode (Fig. S7 in the ESI†).

Different from the structure of **1**, all the E groups linking both Ge_6 rings bend toward the same direction in the basal plane in **2**. Six equatorial Dy^{3+} cations in the $\{Dy_8Ge_{12}\}$ cage exhibit two types of coordination geometries: four Dy^{3+} cations inhabit the bicapped trigonal prism geometries built by two O_{COO} atoms of E groups, four O_{Ge} atoms and two terminal water molecules or one O atom from a CO_3^{2-} anion and one terminal water molecule while the remaining two Dy^{3+} cations adopt the distorted monocapped trigonal prism established by two O_{COO} atoms of E groups, four O_{Ge} atoms and one O atom from the CO_3^{2-} anion (Fig. S8a–c in the ESI†). Both capped Dy^{3+} cations are in eight coordinate bicapped trigonal prism geometries with five O_{Ge}, one O from the E group and one terminal water molecule (Fig. S8d–f in the ESI†). Both supporting eight-coordinate $Dy5^{3+}$ polyhedra are constituted by three O_{COO} atoms of E groups, two O_{CO_3} atoms, two O atoms of the CH_3COO^- anion and one terminal water molecule (Fig. S8g–i in the ESI†). The Dy–O distances are in the range of 2.230(7)–2.609(7) Å, which are comparable with other reported Dy^{3+} compounds.[17] Each $\{Dy_{10}Ge_{12}\}$-**2** SBU links six adjacent same ones *via* E groups in the two-armed face-to-shoulder and single-armed face-to-head modes (Fig. 2e–g), forming the 3D framework with 3D channels along the [100], [010], [011] and [111] directions (Fig. 2h and S9 in the ESI†). The whole framework can be topologically considered as a 6-connected $(4^{12}{\cdot}6^3)$ network by regarding each $\{Dy_{10}Ge_{12}\}$-**2** SBU as a 6-connected node (Fig. 2i).

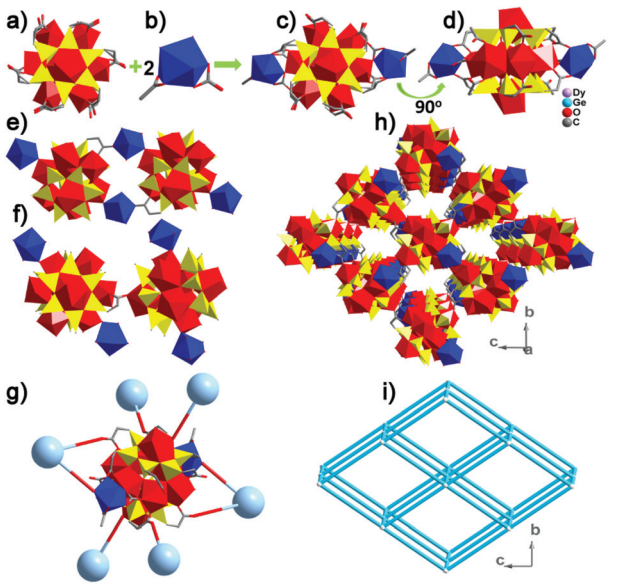

Fig. 2 (a) Top view of the $\{Dy_8Ge_{12}\}$ cage in **2**. (b) View of the $[Dy(CH_3COO)(CO_3)(H_2O)]$ moiety. (c, d) Top and side views of the $\{Dy_{10}Ge_{12}\}$-**2** SBU of **2**. (e, f) The linking modes of neighboring $\{Dy_{10}Ge_{12}\}$-**2** SBUs. (g) The linking mode of each $\{Dy_{10}Ge_{12}\}$-**2** SBU with six adjacent SBUs in **2**. (h) View of the 3D structure of **2** along the [001] direction. (i) Schematic topological view of the 3D framework of **2**.

When we increased the quantity of the second ligand in the reaction system on the basis of Ln salts as the starting materials, fortunately, we obtained two larger clusters consisting of $\{Ln_{10}Ge_{14}\}$-**3**, **4** (Ln = Tb^{3+}, **3**; Dy^{3+}, **4**) SBUs while using 1,2-diaminopropane to adjust the pH of the reaction system, which indicates that the second ligand plays an important role in the formation of **3** and **4**. The $\{Ln_{10}Ge_{14}\}$-**3**, **4** SBUs are formed by bicapped sandwich-type $\{Ln_8Ge_{12}\}$ cages and two supporting $\{LnGeE(HO)_2O(H_2O)(L)\}$ (L = pza^- for **3**; 3-aminopropanoic for **4**) units (Fig. 3a–d and S10 in the ESI†) through one μ_3-O_{Ge} atom, two O_{COO} atoms from E groups and one O_{COO} atom from the pza ligand in **3** (3-aminopropanoic in **4**). Here, the GeO_3E^{2-} moieties in the $[LnGeE(HO)_2O(H_2O)(pza)]$ groups come from the splitting of $H_2E_2Ge_2O_3$ and the 3-aminopropanoic in **4** may come from the decomposition of DL-tyrosine.[18] Because the coordination modes of pza^- ligands in **3** and 3-aminopropanoic in **4** are the same, **3** and **4** have similar structures. Comparable with $\{Dy_{10}Ge_{12}\}$-**2** SBU, for the $\{Ln_{10}Ge_{14}\}$-**3**, **4** SBUs it can be regarded that the CH_3COO^- and CO_3^{2-} groups were replaced by GeO_3E^{2-} and pza^- for **3** (3-aminopropanoic for **4**). However, differently, the CH_3COO^- groups, only as terminal ligands, coordinate to the attached Dy^{3+} cations while the GeO_3E^{2-} moieties act as linkers not only between the bicapped sandwich-type $\{Ln_8Ge_{12}\}$ cage and the supporting Dy^{3+} cations but also between adjacent $\{Ln_{10}Ge_{14}\}$-**3**, **4** SBUs in the $\mu_4{-}\eta^1{:}\eta^2{:}\eta^1{:}\eta^1$ mode (Fig. S11 in the ESI†), resulting in the $\{Dy_8Ge_{12}\}$-**2** cage corner-sharing with the supporting $[Dy(CH_3COO)(CO_3)(H_2O)]$ moiety and the $\{Ln_8Ge_{12}\}$ cage in **3** and **4** edge-sharing with the supporting $\{LnGeE(HO)_2O(H_2O)(L)\}$ groups. Each $\{Ln_{10}Ge_{14}\}$-**3**, **4** SBU combines six adjacent ones, giving rise to 3D LnGeCOFs *via* E groups. Although the bridges between $\{Ln_{10}Ge_{14}\}$-**3**, **4** SBUs are the E groups, there are three and two types of linking modes in **3** and **4**: two-armed head-to-head, two-armed shoulder-to-

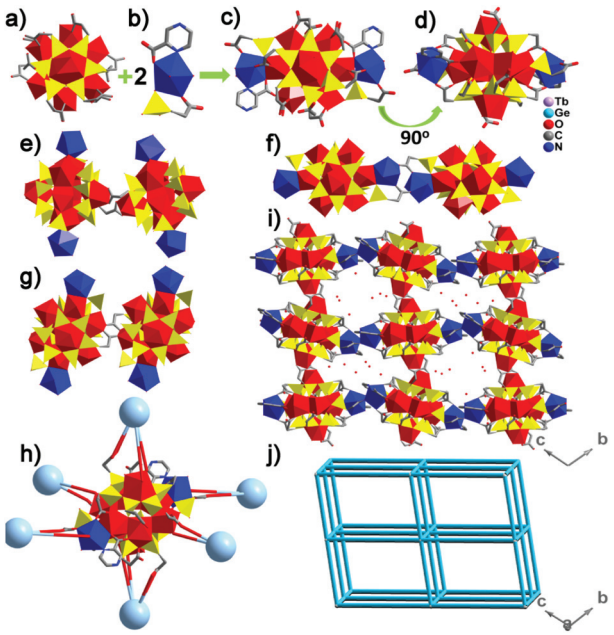

Fig. 3 (a) Top view of the $\{Tb_8Ge_{12}\}$ cage in **3**. (b) View of the $\{TbGeE(HO)_2O(H_2O)(pza)\}$ group. (c, d) The top and side views of the $\{Tb_{10}Ge_{14}\}$-**3** SBU of **3**. (e–g) The linking motifs between neighboring $\{Tb_{10}Ge_{14}\}$-**3** SBUs in **3**. (h) The linking mode of each $\{Tb_{10}Ge_{14}\}$-**3** SBU with six adjacent SBUs. (i) View of the 3D structure of **3** along the [001] direction. (j) Schematic topological view of the 3D framework of **3**.

shoulder and two-armed face-to-face in **3** (Fig. 3e–h); single-armed face-to-head and two-armed shoulder-to-shoulder in **4** (Fig. 4e–g). The LnGeCOF of **3** has 2D channels along the [100] and [111] directions (Fig. 3i and S12 in the ESI†), in which the free water molecules, the pyridyl rings of pza ligands and the organic parts of the E groups point to the inner part of the channels, while LnGeCOF **4** contains 3D channels along the [011] and [100], [010] and [001] directions (Fig. 4h and S13 in the ESI†) with a solvent-accessible volume of 34.6% *via* the PLATON analysis.[19] The whole frameworks of **3** and **4** can be topologically looked on as 6-connected ($4^{12}\cdot6^3$) nets by treating each $\{Ln_{10}Ge_{14}\}$-**3**, **4** SBU as a 6-connected node, respectively (Fig. 3j and 4i).

When the amount of the second ligand (Hpca) in the reaction system was continuously increased, **5** was successfully obtained. The $\{Tb_{11}Ge_{12}\}$-**5** SBU is formed by a bicapped sandwich-type $\{Tb_8Ge_{12}\}$ cage and three supporting $[Tb(pza)_2(H_2O)]^+$ cations (Fig. 5a–d and S14 in the ESI†). From the structural viewpoint, the second ligands in **1–5** only act as connectors between the bicapped sandwich-type $\{Ln_8Ge_{12}\}$ cage and the supporting Ln^{3+} cations, but cannot connect neighboring SBUs. Thus, on continually increasing the amount of the second ligand, **6** was obtained (Fig. 6a–e and S15 in the ESI†), as we expected, the second pza^- ligand links adjacent $\{Dy_{11}Ge_{12}\}$-**6** SBUs together. Single-crystal X-ray diffraction analysis shows that **5** is isostructural to FJ-20.[15] It crystallizes in the cubic space group $I\bar{4}3m$. In the $\{Tb_8Ge_{12}\}$ cage in **5**, E groups bend toward opposite directions in the basal plane. The Tb^{3+} in **5** shows three coordination environments: all six in the equatorial positions are in eight coordinate bicapped trigonal prism geometries *via* four O_{Ge}, two O_{COO} from two E groups and two O_{COO} from two pca ligands, similar to that of

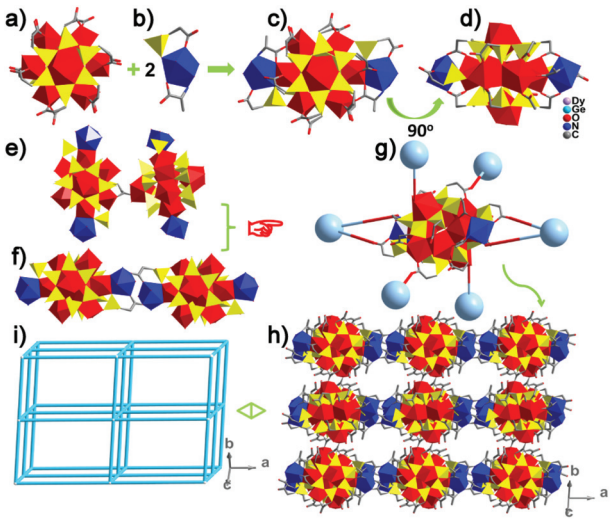

Fig. 4 (a) Top view of the $\{Dy_8Ge_{12}\}$-**4** cage cluster in **4**. (b) View of the $\{DyGeE(HO)_2O(C_3H_5NO_2)(H_2O)\}$ group. (c, d) The top and side views of the $\{Dy_{10}Ge_{14}\}$-**4** SBU of **4**. (e, f) The connection modes of neighboring $\{Dy_{10}Ge_{14}\}$-**4** SBUs in **4**. (g) The combination mode of each $\{Dy_{10}Ge_{14}\}$-**4** SBU with six adjacent SBUs. (h) View of the 3D structure of **4** along the [011] direction. (i) Schematic topological view of the 3D framework of **4**.

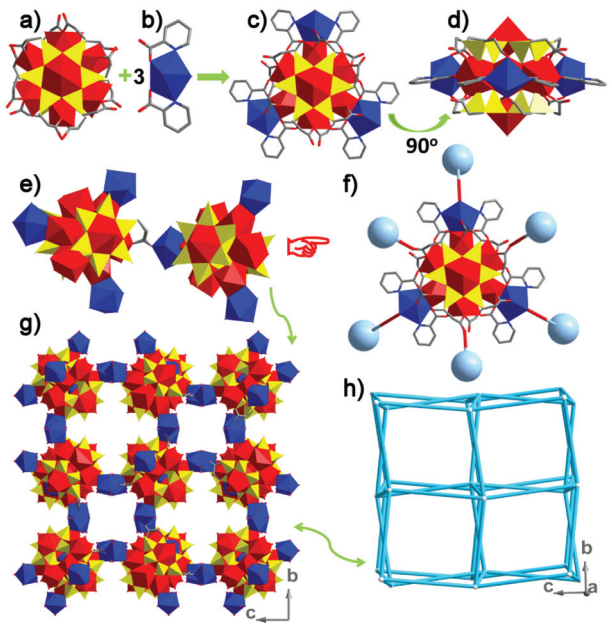

Fig. 5 (a) Top view of the $\{Tb_8Ge_{12}\}$-**5** cage cluster in **5**. (b) View of the $[Tb(pza)_2(H_2O)]^+$ cation. (c, d) Top and side views of the $\{Tb_{11}Ge_{12}\}$-**5** SBU of **5**. (e) The connection modes of neighboring $\{Tb_{11}Ge_{12}\}$-**5** SBUs in **5**. (f) The combination mode of each $\{Tb_{11}Ge_{12}\}$-**5** SBU with six adjacent SBUs. (g) View of the 3D structure of **5** along the [100] direction. (h) Schematic topological view of the 3D framework of **5**.

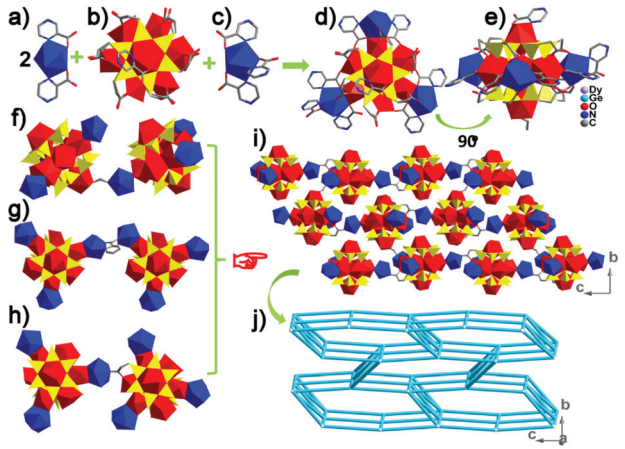

Fig. 6 (a) View of $[Dy(pza)_2(H_2O)]^+$ and $[Dy(pza)_2(H_2O)_2]^+$ cations in **6**. (b) Top view of the $\{Dy_8Ge_{12}\}$ cage cluster in **6**. (c) View of the $[Dy(pza)_3(H_2O)]$ unit in **6**. (d, e) Top and side views of the $\{Dy_{11}Ge_{12}\}$-**6** SBU of **6**. (f–h) The connection modes of neighboring $\{Dy_{11}Ge_{12}\}$-**6** SBUs in **6**. (i) View of the 3D structure of **6** along the [100] direction. (j) Schematic topological view of the 3D framework of **6**.

$Nd6^{3+}$ in **1**; all three attached Tb^{3+} cations are also in eight-coordinate bicapped trigonal prism geometries with three O_{COO} from three E groups, two N and two O_{COO} from two pca ligands and one terminal water molecule; while both capped Tb^{3+} cations inhabit eight-coordinate hexagonal bipyramid geometries *via* six O_{Ge} atoms and two terminal water molecules (Fig. S16 in the ESI†). The Tb–O bond lengths vary from 2.289(8) to 2.757(13) Å and the Tb–N bond length is 2.591(14) Å. Notably, each $\{Tb_{11}Ge_{12}\}$-**5** SBU connects six adjacent ones in the single-armed face-to-shoulder fashion constructing 3D LnGeCOF with the Schläfli symbol of $(4^{12}\cdot6^3)$ (Fig. 5e and f). The framework of **5** contains two types of channels along the [100], [010] and [001] directions, in which the pyridyl rings of pca ligands and the organic parts of the E groups occupy the small and large channels, respectively (Fig. 5g and S17 in the ESI†). The PLATON analysis indicates that the framework has a solvent-accessible volume of 35% for **5**. The $\{Dy_{11}Ge_{12}\}$-**6** SBU is similar to $\{Tb_{11}Ge_{12}\}$-**5** SBU. However, differently, $\{Dy_{11}Ge_{12}\}$-**6** crystallizes in the orthorhombic space group $P2_12_12_1$ and the E groups bend into the same direction in the basal plane. Six equatorial Dy^{3+} cations exhibit three different coordination geometries: the $Dy1^{3+}$ ion employs a seven-coordinate mono-capped trigonal prism geometry constituted by two O_{COO} atoms of E groups, four O_{Ge} atoms and one O_{COO} atom of the pza ligand (Fig. S18a–c in the ESI†); the $Dy2^{3+}$, $Dy3^{3+}$, $Dy4^{3+}$ and $Dy6^{3+}$ ions exhibit eight-coordinate bicapped trigonal prism geometries and have the same coordination environments as the equatorial Tb^{3+} cation in the $\{Tb_8Ge_{12}\}$ cluster in **5**; the $Dy5^{3+}$ ion dwells in a nine-coordinate tricapped trigonal prism geometry defined by two O_{COO} atoms of E groups, four O_{Ge} atoms, two O_{COO} atom of pza ligands and one terminal water molecule (Fig. S18d–f in the ESI†).

Although both capped Dy^{3+} cations in two polar positions of the $\{Dy_8Ge_{12}\}$ cluster in **6** show ten-coordinate capped triangular cupola geometries but have different coordination environments: the $Dy7^{3+}$ ion links to six O_{Ge} atoms, one O atom and one N atom of the pza ligand and two terminal water molecules (Fig. S18g–i in the ESI†); the $Dy8^{3+}$ ion is coordinated by six O_{Ge} atoms, one O_{COO} atom of the $HCOO^-$ anion and three water molecules (Fig. S18j–l in the ESI†). Three supporting Dy^{3+} cations in the $\{Dy_8Ge_{12}\}$ cage in **6** all are bedded in nine-coordinate tricapped trigonal prism geometries but also have different coordination environments: the $Dy9^{3+}$ ion possesses the same coordination environment as the supporting Tb^{3+} cations in the $\{Tb_8Ge_{12}\}$ cluster in **5**; the $Dy10^{3+}$ ion is combined with two O_{COO} atoms of E groups, three O_{COO} atoms and two N atoms of pza ligands, one O_{COO} atom of the $HCOO^-$ anion and one terminal water molecule (Fig. S18m–o in the ESI†); the $Dy11^{3+}$ ion is coordinated by two O_{COO} atoms of E groups, three O_{COO} atoms and three N atoms of pza ligands and one terminal water molecule (Fig. S18p–r in the ESI†). The pza ligand bonded to the $Dy11^{3+}$ ion links adjacent $\{Dy_{11}Ge_{12}\}$-**6** SBUs. The Dy–O and Dy–N distances range from 2.313(7) to 2.772(8) Å and 2.615(12) to 2.741(10) Å, respectively. There are three kinds of linkers between neighboring $\{Dy_{11}Ge_{12}\}$-**6** SBUs: the E groups, the pza ligands and the $HCOO^-$ groups (Fig. 6f–h). Each $\{Dy_{11}Ge_{12}\}$-**6** SBU also combines six neighboring ones (Fig. S19 in the ESI†) giving rise to 3D LnGeCOF with 3D channels along the [100], [001] and [110] directions (Fig. 6i and S20 in the ESI†), in which the pyridyl rings of pza^- ligands and the organic parts of the E groups are located in the inner part of the channels. The whole framework of **6** can be topologically simplified as a 6-connected network with the Schläfli symbol of $(3^3\cdot4^6\cdot5^5\cdot6)$ (Fig. 6j).

PXRD patterns and thermal stability

In order to identify the phase purity of **1–6**, their PXRD patterns have been recorded. The consistency of the PXRD patterns of the bulks and the calculated patterns from the single-crystal structural analyses proves the good phase purity of **1–6** (Fig. S21 in the ESI†).

To investigate the thermal stability of **1–6**, their thermogravimetric (TG) analyses have been investigated in a dry air atmosphere from 30 to 1000 °C at a heating rate of 10 °C min^{-1} (Fig. S22 in the ESI†). **1**, **2**, **3** and **4** display three steps of weight loss between 30 and 1000 °C. The first-step weight loss of 8.44% in the range of 30–335 °C for **1** corresponds to the removal of three lattice water molecules and thirteen coordinated water molecules (calcd 7.07%); 10.94% in the range of 30–298 °C for **2** is assigned to the removal of eleven lattice water molecules and fourteen coordinated water molecules before 298 °C (calcd 10.16%); 10.80% (calcd 11.14%) between 30 and 378 °C is owing to the release of eighteen lattice water molecules and eight coordinated water molecules for **3**; and 8.14% in the range of 30–264 °C for **4** is attributed to the removal of eight lattice water molecules, twelve coordinated water molecules and four hydroxylic groups (calcd 8.47%). The observed weight loss for **1** is slightly higher than the calculated value, which can be attributed to the loss of the adsorbed

water.[20] The remaining two steps of weight loss are mainly attributable to the removal of organic groups. Assuming that the residue of **1** corresponds to $4.5Nd_2O_3{\cdot}12GeO_2$ ($5Dy_2O_3{\cdot}12GeO_2$ for **2**; $5Tb_2O_3{\cdot}14GeO_2$ for **3** and $5Dy_2O_3{\cdot}14GeO_2$ for **4**), the observed total weight (67.99% for **1**; 69.51% for **2**; 68.69% for **3** and 71.86% for **4**) is in good agreement with the calculated value (67.95% for **1**; 70.38% for **2**; 68.43% for **3** and 71.91% for **4**). **5** and **6** have similar TG curves, displaying four major steps of weight loss. The first weight loss of 7.26% (calcd 7.22%) between 30 and 322 °C corresponds to the loss of ten lattice water molecules, three hydroxyl groups and seven coordinated water molecules for **5**; 4.48% (calcd 5.19%) between 30 and 279 °C corresponds to the loss of five lattice water molecules and ten coordinated water molecules for **6**. Then the framework was decomposed, which is attributed to the departure of organic groups. Assuming that the residue of **5** and **6** corresponds to $5.5Ln_2O_3{\cdot}12GeO_2$ (Ln = Tb^{3+} for **5**; Dy^{3+} for **6**), the observed total weight of 62.51% for **5** (64.08% for **6**) is in good agreement with the calculated value 62.67% for **5** (64.07% for **6**).

Photoluminescence (PL) properties

Ln^{3+} cations with their unique electronic structures usually manifest an efficient emission ability ranging from UV-Visible to the near infrared region,[21] which endows Ln^{3+} activated luminescent materials with wide applications in photonic devices such as optical amplifiers, laser materials, luminescent probes and flat displays.[22] For the sake of studying PL properties, the excitation spectra, emission spectra and lifetime decay behaviors of **1**, **3** and **5** have been investigated with crystalline samples upon photoexcitation at ambient temperature. Upon excitation at 587 nm, the luminescence spectrum of **1** in the 800–1500 nm near IR region consists of three emission peaks at 898, 1062 and 1337 nm, which correspond to the expected f–f transitions ($^4F_{3/2} \rightarrow {}^4I_{9/2}$, $^4F_{3/2} \rightarrow {}^4I_{11/2}$ and $^4F_{3/2} \rightarrow {}^4I_{13/2}$) of the Nd^{3+} cation (Fig. 7a).[23] The excitation spectrum of **1** is collected by monitoring the most intense emission peak at 1062 nm and shows three apparent transition peaks from the $^4I_{9/2}$ ground-states to various excited states of the Nd^{3+} cation (Fig. S23 in the ESI†).[24] When **3** is excited under the ultraviolet light of 277 nm, a green emission is observed with accompanying seven characteristic luminescent emission bands with maxima at 494, 543, 586, 623, 681, 669 and 647 nm in the PL spectrum (Fig. 7b), which are assigned to transitions from the $^5D_4$ excited-state to lower ^7F_J levels, namely, the $^5D_4 \rightarrow {}^7F_6$ (494 nm), $^5D_4 \rightarrow {}^7F_5$ (543 nm), $^5D_4 \rightarrow {}^7F_4$ (586 nm), $^5D_4 \rightarrow {}^7F_3$ (623 nm), $^5D_4 \rightarrow {}^7F_2$ (681 nm), $^5D_4 \rightarrow {}^7F_1$ (669 nm) and $^5D_4 \rightarrow {}^7F_0$ (647 nm) transitions of the Tb^{3+} cation.[25] Similarly, **5** emits green PL upon the excitation of 302 nm and the emission spectrum also displays seven characteristic emission bands with maxima at 493, 543, 586, 681, 669 and 650 nm (Fig. 7c) that are derived from the $^5D_4$ excited state of the Tb^{3+} cation to the ground state ^7F_J manifold (J = 6, 5, 4, 3, 2, 1, 0). The most intense emission band at 543 nm for **3** and **5** is the $^5D_4 \rightarrow {}^7F_5$ transition. By monitoring the $^5D_4 \rightarrow {}^7F_5$ emission at 543 nm, the excitation spectra of **3** and **5** are also collected in Fig. S24.† In addition, the luminescent decay curves of **1**, **3** and **5** are taken by monitoring the most intense emission band (λ_{ex} = 587 nm, λ_{em} = 1062 nm for **1**; λ_{ex} = 277 nm, λ_{em} = 543 nm for **3**; λ_{ex} = 302 nm, λ_{em} = 543 nm for **5**, Fig. 7d–f). All the lumine-

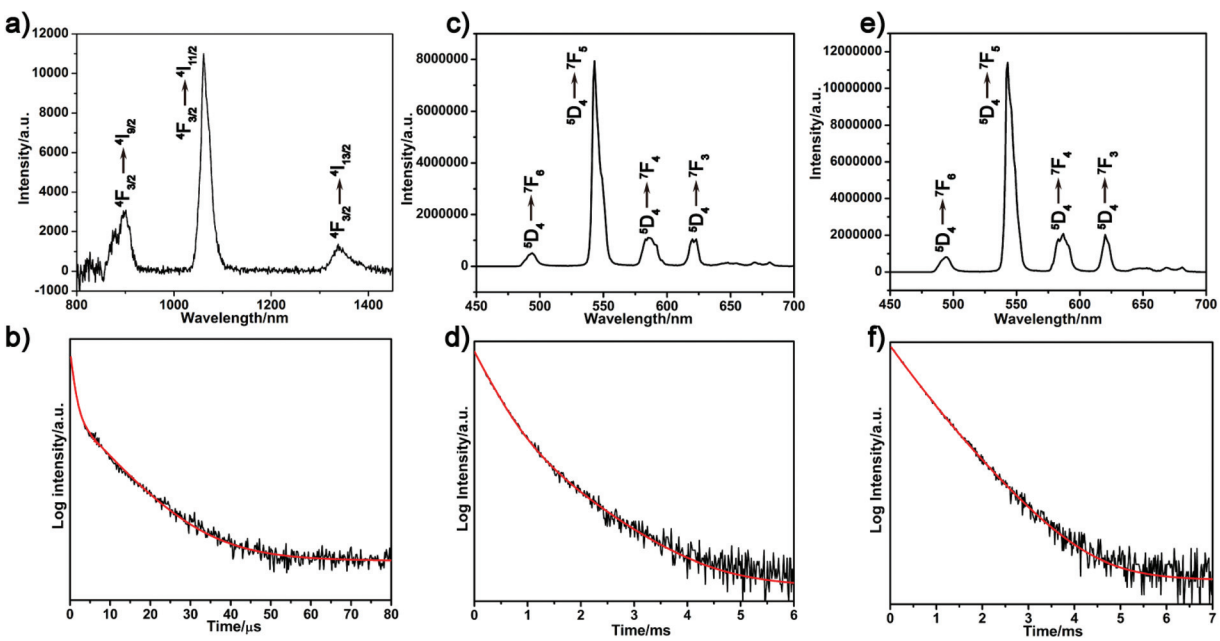

Fig. 7 (a) The solid-state PL spectrum of **1** under excitation at 587 nm at room temperature. (b) The solid-state PL spectrum of **3** under excitation at 277 nm at room temperature. (c) The solid-state PL spectrum of **5** under excitation at 302 nm at room temperature. (d) The luminescence decay curve of **1** with the double-exponential behavior. (e) The luminescence decay curve of **3** with the double-exponential behavior. (f) The luminescence decay curve of **5** with the double-exponential behavior.

scent decay curves can be well fitted to the double-exponential function as $I = A_1 \exp(-t/\tau_1) + A_2 \exp(-t/\tau_2)$ (A_1 and A_2 represent pre-exponential factors whereas τ_1 and τ_2 represent the fast and slow components of the luminescence lifetimes), affording τ_1 = 1.02 μs (22.85%), τ_2 = 10.14 μs (77.15%), A_1 = 4643.10, A_2 = 1577.72 for **1**, τ_1 = 294.04 μs (69.72%), τ_2 = 830.18 μs (30.28%), A_1 = 5344.75, A_2 = 822.31 for **3** and τ_1 = 551.87 μs (47.31%), τ_2 = 902.46 μs (52.69%), A_1 = 4194.12, A_2 = 2855.93 for **5**. Based on $\tau = (A_1\tau_1^2 + A_2\tau_2^2)/(A_1\tau_1 + A_2\tau_2)$,[26] the average lifetimes of **1**, **3** and **5** can be calculated to be 8.08 μs, 456.40 μs and 736.58 μs, respectively. Obviously, **1**, **3** and **5** exhibit the Ln-centered characteristic emission.

Conclusions

In summary, six novel LnGeCOFs derived from bicapped sandwich-type $\{Ln_8Ge_{12}\}$ cage clusters **1–6** have been successfully prepared under mild hydrothermal conditions using an organogermanium bis(carboxyethylgermanium)sesquioxide as a starting material. The structural assembly from $\{Nd_9Ge_{12}\}$-**1** to $\{Ln_{11}Ge_{12}\}$-**5**, **6** (Ln = Tb^{3+}, **5**; Dy^{3+}, **6**) based on Ln oxides as the Ln sources and the structural assembly from $\{Dy_{10}Ge_{12}\}$-**2** to $\{Ln_{10}Ge_{14}\}$-**3**, **4** (Ln = Tb^{3+}, **3**; Dy^{3+}, **4**) based on Ln salts as the Ln sources can indicate that the amount of the second ligands plays an important role in the structural construction of **1–6**. Furthermore, the photoluminescence measurements show that **1** exhibits the characteristic near infrared emission of the Nd^{3+} cation and **3** and **5** display the characteristic visible emission of the Tb^{3+} cation. Their fluorescence lifetimes have also been measured. In further work, we will concentrate on judiciously selecting suitable *N*-containing multi-carboxylic ligands to prepare novel organic–inorganic hybrid LnGeCOF materials and systematically investigate their adsorption, magnetic and optical properties.

Acknowledgements

This work was supported by the NSFC (no. 21571016 and 91122028), and the NSFC for Distinguished Young Scholars (no. 20725101).

References

1 (*a*) J. Sun, C. Bonneau, A. Cantin, A. Corma, M. J. Diaz-Cabanas, M. Moliner, D. Zhang, M. Li and X. Zou, *Nature*, 2009, **458**, 1154–1157; (*b*) M. E. Davis, *Nature*, 2002, **417**, 813–821; (*c*) C. Y. Pan, G. Z. Liu, S. T. Zheng and G. Y. Yang, *Chem. – Eur. J.*, 2008, **14**, 5057–5063.

2 (*a*) T. Yokoi, M. Yoshioka, H. Imai and T. Tatsumi, *Angew. Chem., Int. Ed.*, 2009, **48**, 9884–9887; (*b*) K. Itabashi, Y. Kamimura, K. Iyoki, A. Shimojima and T. Okubo, *J. Am. Chem. Soc.*, 2012, **134**, 11542–11549; (*c*) S. Inagaki, Y. Tsuboi, Y. Nishita, T. Syahylah, T. Wakihara and Y. Kubota, *Chem. – Eur. J.*, 2013, **19**, 7780–7786.

3 (*a*) N. Guillou, Q. Gao, P. M. Forster, J. S. Chang, M. Nogues, S. E. Park, G. Ferey and A. K. Cheetham, *Angew. Chem., Int. Ed.*, 2001, **40**, 2831–2834; (*b*) C. H. Lin, S. L. Wang and K. H. Lii, *J. Am. Chem. Soc.*, 2001, **123**, 4649–4650; (*c*) C. M. Wang, L. W. Lee, T. Y. Chang, Y. C. Chen, H. M. Lin, K. L. Lu and K. H. Lii, *Chem. – Eur. J.*, 2015, **21**, 1878–1881.

4 (*a*) X. Zou, T. Conradsson, M. Klingstedt, M. S. Dadachov and M. O'Keeffe, *Nature*, 2005, **437**, 716–719; (*b*) L. Tang, M. S. Dadachov and X. Zou, *Chem. Mater.*, 2005, **17**, 2530–2536; (*c*) Z. E. Lin, J. Zhang, J. T. Zhao, S. T. Zheng, C. Y. Pan, G. M. Wang and G. Y. Yang, *Angew. Chem., Int. Ed.*, 2005, **44**, 6881–6884; (*d*) J. Liang, J. Su, Y. Wang, Y. Chen, X. Zou, F. Liao, J. Lin and J. Sun, *Chem. – Eur. J.*, 2014, **20**, 16097–16101.

5 (*a*) M. O'Keeffe, M. Eddaoudi, H. Li, T. Reineke and O. M. Yaghi, *J. Solid State Chem.*, 2000, **152**, 3–20; (*b*) G. Férey, *J. Solid State Chem.*, 2000, **152**, 37–48; (*c*) G. Férey, C. Mellot Draznieks and T. Loiseau, *Solid State Sci.*, 2003, **5**, 79–94.

6 (*a*) G. Z. Liu, H. X. Zhang, Z. E. Lin, S. T. Zheng, J. Zhang, J. T. Zhao, G. M. Wang and G. Y. Yang, *Chem. – Asian J.*, 2007, **2**, 1230–1239; (*b*) Q. Pan, J. Li, K. E. Christensen, C. Bonneau, X. Ren, L. Shi, J. Sun, X. Zou, G. Li, J. Yu and R. Xu, *Angew. Chem., Int. Ed.*, 2008, **47**, 7868–7871.

7 (*a*) Z. E. Lin, S. T. Zheng and G. Y. Yang, *Z. Anorg. Allg. Chem.*, 2006, **632**, 354–358; (*b*) L. Tang, L. Shi, C. Bonneau, J. Sun, H. Yue, A. Ojuva, B. L. Lee, M. Kritikos, R. G. Bell, Z. Bacsik, J. Mink and X. Zou, *Nat. Mater.*, 2008, **7**, 381–385.

8 (*a*) Z. E. Lin, J. Zhang, S. T. Zheng and G. Y. Yang, *Microporous Mesoporous Mater.*, 2004, **74**, 205–211; (*b*) Y. Zhou, H. Zhu, Z. Chen, M. Chen, Y. Xu, H. Zhang and D. Zhao, *Angew. Chem., Int. Ed.*, 2001, **40**, 2166–2168; (*c*) M. P. Attfield, Y. A. Ebini, R. G. Pritchard, E. M. Andrews, R. J. Charlesworth, W. Hung, B. J. Masheder and D. S. Royal, *Chem. Mater.*, 2007, **19**, 316–322.

9 (*a*) M. E. Medina, E. Gutierrez-Puebla, M. A. Monge and N. Snejko, *Chem. Commun.*, 2004, 2868–2869; (*b*) K. E. Christensen, C. Bonneau, M. Gustafsson, L. Shi, J. Sun, J. Grins, K. Jansson, I. Sbille, B. L. Su and X. Zou, *J. Am. Chem. Soc.*, 2008, **130**, 3758–3759.

10 M. Emirdag-Eanes and Z. Kristallogr, *New Cryst. Struct.*, 2002, **217**, 17–18.

11 P. L. Chen, P. Y. Chiang, H. C. Yeh, B. C. Chang and K. H. Lii, *Dalton Trans.*, 2008, 1721–1726.

12 W. Liu, M. Yang, Y. Ji, F. Liu, Y. Wang, X. Wang, X. Zhao and X. Liu, *RSC Adv.*, 2014, **4**, 26951–26955.

13 (*a*) X. Zhao, T. Yan, K. Wang, Y. Yan, B. Zou, J. Yu and R. Xu, *Eur. J. Inorg. Chem.*, 2012, 2527–2532; (*b*) X. Wang, Y. Wang, Q. Liu, Y. Li, J. Yu and R. Xu, *Inorg. Chem.*, 2012, **51**, 4779–4783.

14 (*a*) G. J. C. Bunzli and C. Piguet, *Chem. Soc. Rev.*, 2005, **34**, 1048–1077; (*b*) J. G. Mao, *Coord. Chem. Rev.*, 2007, **251**, 1493; (*c*) C. M. Wang, Y. Y. Wu, Y. W. Chang and K. H. Lii, *Chem. Mater.*, 2008, **20**, 2857–2859.

15 H. He, G. J. Cao, S. T. Zheng and G. Y. Yang, *J. Am. Chem. Soc.*, 2009, **131**, 15588–15589.
16 (*a*) G. M. Sheldrick, *SHELXL-97, Program for Structure Refinement*, University of Göttingen, Göttingen, Germany, 1997; (*b*) G. M. Sheldrick, *SHELXS-97, Program for Structure Solution*, University of Göttingen, Göttingen, Germany, 1999.
17 S. X. She, Y. M. Chen, M. J. Zaworotko, W. Liu, Y. Y. Cao, J. Wu and Y. H. Li, *Dalton Trans.*, 2013, **42**, 10433–10488.
18 I. Ntai, V. V. Phelan and B. O. Bachmann, *Chem. Commun.*, 2006, 4518–4520.
19 A. L. Spek, *Acta Crystallogr., Sect. A: Fundam. Crystallogr.*, 1990, **46**, 194–201.
20 D. B. Xiong, J. T. Zhao, H. H. Chen and X. X. Yang, *Chem. – Eur. J.*, 2007, **13**, 9862–9865.
21 Y. S. Liu, D. T. Tu, H. M. Zhua and X. Y. n Chen, *Chem. Soc. Rev.*, 2013, **42**, 6924–6958.
22 (*a*) K. Kuriki, Y. Koike and Y. Okamoto, *Chem. Rev.*, 2002, **102**, 2347–2356; (*b*) J. Kido and Y. Okamoto, *Chem. Rev.*, 2002, **102**, 2357–2368; (*c*) V. J. Pansare, S. Hejazi, W. J. Faenza and R. K. Prud'homme, *Chem. Mater.*, 2012, **24**, 812–827; (*d*) X. L. Sun, B. X. Shen, S. Q. Zang and C. X. Du, *CrystEngComm*, 2013, **15**, 5910–5918.
23 P. C. R. Soares-Santos, L. S. Cunha-Silva, F. A. A. Paz, R. A. S. Ferreira, J. Rocha, L. S. D. Carlos and H. I. S. Nogueira, *Inorg. Chem.*, 2010, **49**, 3428–3440.
24 P. C. R. Soares-Santos, L. Cunha-Silva, F. A. Almeida Paz, R. A. S. Ferreira, J. Rocha, L. D. Carlos and H. I. S. Nogueira, *Inorg. Chem.*, 2010, **49**, 3428–3440.
25 C. Ritchie, V. Baslon, E. G. Moore, C. Reber and C. Boskovic, *Inorg. Chem.*, 2012, **51**, 1142–1151.
26 J. Zhou and Z. G. Xia, *J. Mater. Chem. C*, 2015, **3**, 7552–7560.